Influence of the Microplasma Actuator Electrode Configuration on the Induced EHD Flow

Marius Blajan, Daisuke Nonanka, Jaroslav Kristof and Kazuo Shimizu
Organization for Innovation and Social Collaboration
Shizuoka University, Nakaku, Johoku, Hamamatsu, 432-8561, Japan
phone: (+81) 53-478-1443
e-mail: blajanmarius@yahoo.com, js32rz47@gmail.com, jaroslav.kristof@gmail.com, shimizu@cjr.shizuoka.ac.jp

***Abstract*— A microplasma actuator was developed for the flow control applications. It is a type of dielectric barrier discharge plasma actuator that due to its simple construction and no moving parts has advantages over the mechanical type of actuators used for flow control. Numerical simulations were carried out in order to analyze the induced Electro Hydro Dynamic (EHD) flow. The microplasma actuator has a thin dielectric layer with a thickness of 25 μm between the grounded and high voltage energized electrodes thus the discharge voltage is about 1 kV. The high voltage electrodes consist of alternating strip-like electrodes that are placed above a plate-like electrode with the dielectric layer in between. In the series of experiments an AC voltage with amplitude 1.4 kV and 20 kHz was applied to the electrodes. A parametric study was carried out in which the number of strip-like electrodes was varied. Thus four and eight strip-like electrodes were used and their influence on the induced EHD flow was analyzed. With the increase in the number of strip-like electrodes the maximum values of the induced flow increased.**

I. Introduction

Active flow control used in industrial processes improves the system efficiency and reduces the environmental load [1]. The flow control is achieved in classical way by using mechanical actuators. A new flow control device was developed in the 1990s by Roth *et al.* and it was called *plasma actuator* [2]. A dielectric barrier discharge (DBD) was used as the actuator. This atmospheric nonthermal plasma actuator for flow control has advantages over the classical mechanical actuators such as no moving parts, simple construction, and high-frequency response [3], [4]. Applications such as flow control [5]–[8] and noise reduction [9], [10] were investigated by various research groups. The plasma actuator has and operating principle based on the electrohydrodynamic (EHD) phenomenon occurring due to the momentum transfer from ions accelerated by electric field to neutral molecules by collision. Microplasma actuators have small dimensions thus experimental investigation and measurements are difficult to carry out thus numerical simulations could add valuable insights. A simulation code based on the Suzen & Huang [11-12] and Orlov [13]

models, was developed. The flow near the active electrodes is difficult to measure for the microplasma actuator due to the light emission of plasma thus numerical simulations were carried out. There are various algorithms and method for the simulation of plasma actuators, among them plasma fluid model and particle in cell model [14-17]. The Suzen-Huang model is a simplified phenomenological model which does not model the species transport equations but can replicate the effects of the actuator on the air [18]. Various researcher validated the algorithm by obtaining numerical simulation results close to the experimental ones [18]-[19]. One advantage of this algorithm is that is computational less expensive than solving the species transport equations.

II. Microplasma Actuator

Despite the requirement of low discharge voltage, the micro scale plasma actuator has the advantage of easy integration due to its small size. The developed DBD microplasma actuator is described in [20].

Due to the microscale gap, a high electric field (10^7~10^8 V/m) could be obtained at the topside electrode by application of a voltage of 1.4 kV. Such a low voltage is easy to insulate or control and contributes to the miniaturization of the system. Moreover, due to the use of the resin film, which is a lightweight and flexible polymer, the plasma actuator could be attached to surfaces of different shapes making it ideal for the flow control.

Based on the characteristics of the microplasma actuator numerical simulations were carried out using a similar geometry. The electrodes positioned in the left part of the actuator ($x<0$) are defined as HV1 and HV2 while the electrodes on the right part ($x>0$) were defined as HV3 and HV4, as shown in Figure 1. The electrodes that were covered by the dielectric layer were grounded.

III. Numerical Simulation of Microplasma Actuator

The numerical simulation was carried out to study the influence of the microplasma electrode configuration on the induced flow.

A. Simulation algorithm

The simulation was carried out using a model developed by Suzen [11]–[12]. The description of the algorithm which uses Suzen model coupled with Navier-Stokes equations is given in [11]-[12], [19] and [21].

The computational geometry is shown in Fig. 1. The dimensions of the grid were 11.5 x 11.5 mm with 461 x 461 grid nodes. Convergence parameter for solving (7) and (10) was 10^{-8}. In this study only 8 exposed electrodes and 4 covered electrodes were considered as shown in Fig. 1. The value of the source charge was considered $\rho c = 0.00752$ C/m^3 .The exposed electrodes were labeled HV1 (2 electrodes), HV2 (2 electrodes), HV3 (2 electrodes) and HV4 (2 electrodes). The numerical simulations were carried out by energizing the exposed electrodes at an AC waveform having amplitude 1.4 kV and 20 kHz.

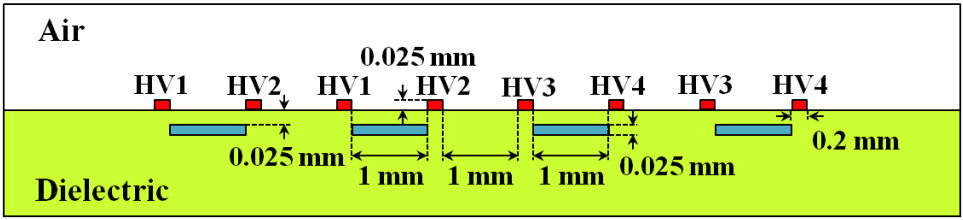

Fig. 1. Computational geometry. HV2 and HV4 were energized for the leftward flow and HV1 and HV4 were energized for upward flow. The electrodes encapsulated in dielectric were at 0 V potential.

The permittivity of the dielectric layer was ε_{rd} =4 and in between dielectric and air was considered the harmonic mean between the dielectric permittivity and air permittivity εr_{air} = 1 thus the electric field was conserved. The source charge was investigated as a parameter.

B. Influence of charge parameter on the induced flow

The finite difference method was used for the discretization of the equations, which were computed before solving the Navier-Stokes equations. The maximum values of the external electric field, charge, and furthermore body force are shown in Fig. 2. The highest intensity of body force was obtained near the active exposed electrodes HV1, HV2, and HV4 above the grounded electrodes. Julia programming language was used to write the simulation program. The Navier-Stokes equations were solved using the projection method in primitive variables on a collocated mesh. The time step was 2 μs. The simulation conditions were similar with the experimental ones: thus, up to 50 ms, the energized electrodes were HV2 and HV4, and after 50 ms, the energized electrodes were HV1 and HV4. In Fig. 3, the simulation results are shown when the energized electrodes were HV2 and HV4. The initial stages of the phenomenon are shown at 2 ms.

The vortexes that appeared above the covered electrode had a clockwise direction. At time t=8 ms the vortexes start to break and unite. At 20 ms the flow is flattened and a leftward flow is created. The induced flow at 50 ms is at steady state. The calculated flow speed was approximately 0.9 m/s in some regions above the grounded electrode and approximately 0.8 m/s in the left region where the leftward flow widened. The experimental data from [21] showed same pattern for the induced flow using the multi-electrode system microplasma actuator. The experimental results from [21] above the electrode were difficult to measure due to the light emission of microplasma which interfered with the Particle tracking velocimetry (PTV) measurement method thus the numerical simulation could give us additional information about the flow.

In Figure 4, the simulation results when the energized electrodes were HV1 and HV4 are shown. After 50 ms, the configuration of energized electrodes was changed, thus leftward flow above the HV1 electrodes changed to counter-clockwise vortexes. At 60 ms two big vortexes are developed and at 64 ms the vortexes start to unite.

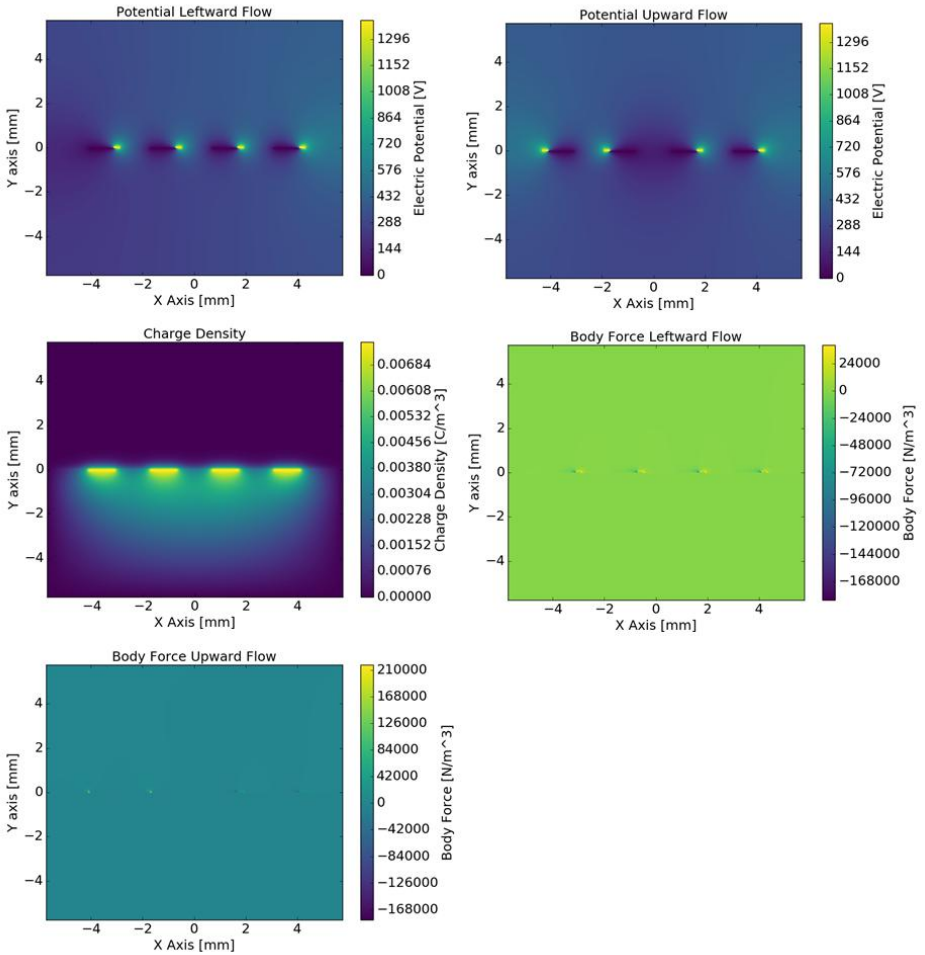

Fig. 2. Electric potential, charge density and body force for 8 electrodes arrangement: Exposed electrodes HV=1400V; Encapsulated electrodes=0 V. Potential Leftward Flow shows the potential for the setup with active electrodes HV2 and HV4. Potential Upward Flow shows the potential for the setup with active electrodes HV1 and HV4. Charge Density shows the charge density for all setups. Body Force Leftward Flow shows the body force for the setup with active electrodes HV2 and HV4. Body Force Upward Flow shows the body force for the setup with active electrodes HV1 and HV4.

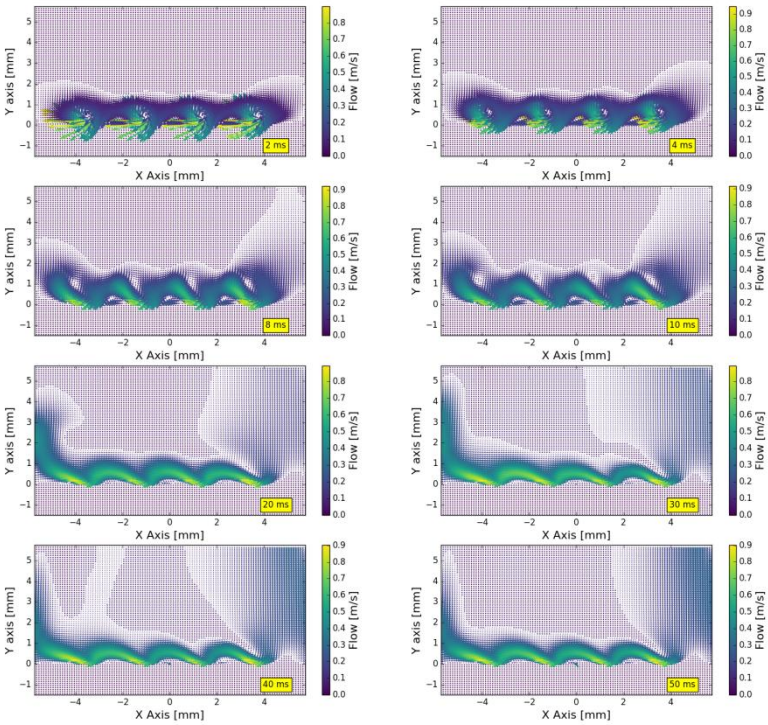

Fig. 3. Flow up to 50 ms for 8 electrodes arrangement. Electrodes HV2 and HV4 were energized at 1.4 kV.

After 74 ms, the vortexes unite and form a single bigger vortex. The vortex gradually moves upward, and an upward flow is also obtained in the centre region due to the flow from the HV4 electrodes. The calculated flow speed in the regions above the grounded electrodes was approximately 1.08 m/s, and approximately 0.91 m/s in the centre region.

The change in the induced flow direction is necessary when applying the microplasma actuator for flow control and it can be achieved using semiconductor switches.

After achieving a steady state while energizing electrodes HV2 and HV4, the configuration of the microplasma actuator was changed to HV1 and HV4 as the electrodes energized, a longer time was required to achieve a steady state for the upward flow. Thus, as shown in Figure 4 the steady state for the upward flow was achieved at approximately 120 ms.

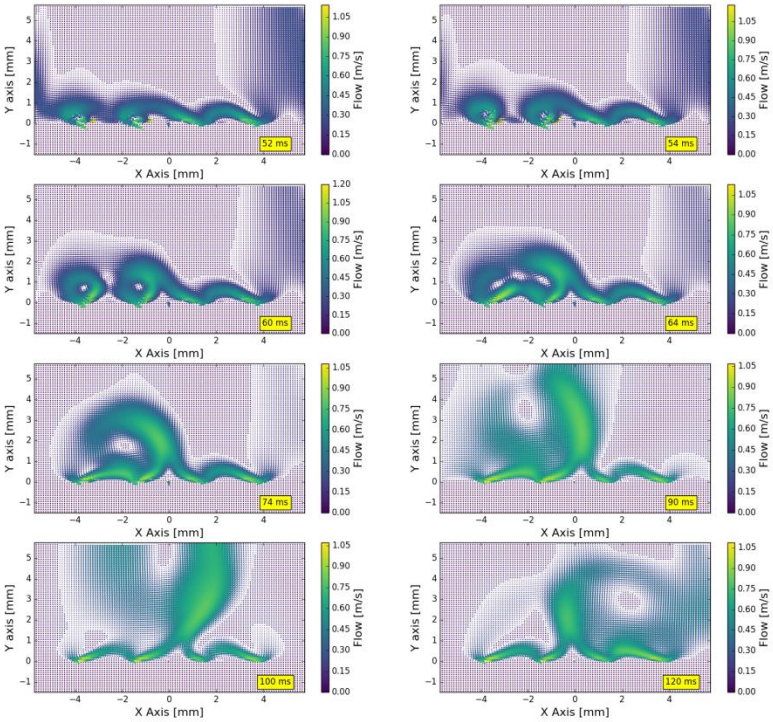

Fig. 4. Flow up to 120 ms for 8 electrodes arrangement. Electrodes HV1 and HV4 were energized at 1.4 kV.

The simulation were carried out for the values of the source charge ρc = 0.00750 C/m^3, 0.00751 C/m^3 and 0.00752 C/m^3.

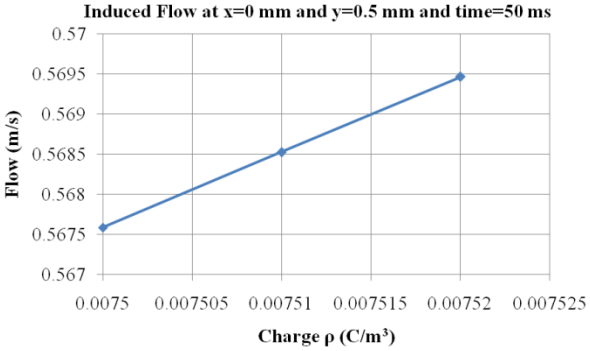

Fig. 5. Induced flow for various values of source charge at 50 ms and x=0 mm and y=0.5 mm.

The source charge ρc used by Suzen [12] was 0.0075 C/m^3.This parameter should be calibrated with the experimental data. The results presented in [21] showed a good fit for ρc = 0.00751 C/m^3 but according to Fig. 5 and Fig. 6 a better fit with the experimental data is for the value of ρc = 0.00752 C/m^3.

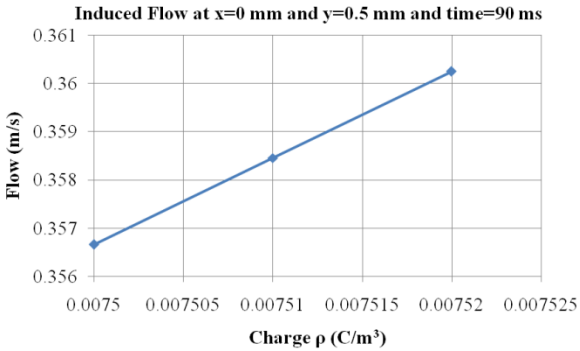

Fig. 6. Induced flow for various values of source charge at 90 ms and x=0 mm and y=0.5 mm.

At 50 ms and x=0 mm and y=0.5 mm the values of the induced flow were calculated to be between 0.5675 m/s to 0.5695 m/s. At 90 ms and x=0 mm and y=0.5 mm the values were between 0.3568 m/s and 0.3602 m/s.

C. Influence of the electrode configuration on the induced flow

The influence of the number of electrodes on flow pattern was investigated thus besides the 8 electrodes configuration results which were shown in previous chapter also a configuration with 4 electrodes was simulated. The maximum values of the external electric field, charge, and furthermore body force are shown in Fig. 7. The highest intensity of body force was obtained near the active exposed electrodes HV1, HV2, and HV4 above the grounded electrodes. The simulation conditions were same as 8 electrodes configuration with the experimental ones: thus, up to 50 ms, the energized electrodes were HV2 and HV4, and after 50 ms, the energized electrodes were HV1 and HV4. In Fig. 8, the simulation results are shown when the energized electrodes were HV2 and HV4. The initial stages of the phenomenon are shown at 2 ms.

The vortexes that appeared above the covered electrode had a clockwise direction and maintained their vortex shape up to 8 ms. At time t=10 ms the vortexes start to break and join together. At 20 ms the leftward flow is obtained. Up to 50 ms the induced flow is extended and flattened towards the left part of the actuator. The results at 50 ms appear to be a steady state which was also observed in the experiments. The calculated flow speed was approximately 0.89 m/s in some regions above the grounded electrode and approximately 0.6 m/s in the left region where the leftward flow widened. The leftward flow established after 50 ms had similar pattern with was observed for the 8 electrodes configuration but the values were slightly lower than in the case of 8 electrodes configuration.

In Fig. 9, the simulation results when the energized electrodes were HV1 and HV4 are shown. After 50 ms, the configuration of energized electrodes was changed, thus leftward flow above the HV1 electrode changed to a counter-clockwise vortex.

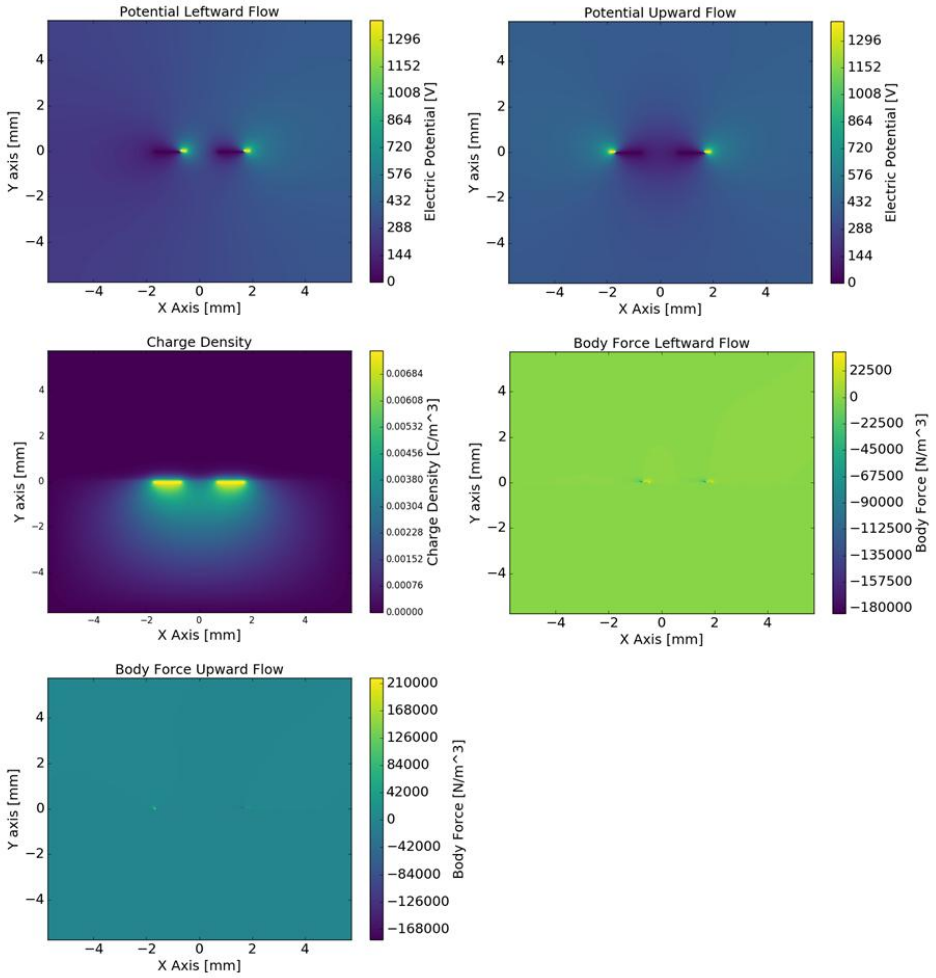

Fig. 7. Electric potential, charge density and body force for 4 electrodes arrangement: Exposed electrodes HV=1400V; Encapsulated electrodes=0 V. Potential Leftward Flow shows the potential for the setup with active electrodes HV2 and HV4. Potential Upward Flow shows the potential for the setup with active electrodes HV1 and HV4. Charge Density shows the charge density for all setups. Body Force Leftward Flow shows the body force for the setup with active electrodes HV2 and HV4. Body Force Upward Flow shows the body force for the setup with active electrodes HV1 and HV4.

The vortex increased in size until 90 ms when the vortex starts to break and move upward thus with the flow induced by the HV4 electrode an upward flow in center of the actuator was obtained. The calculated flow speed in the regions above the grounded electrodes was approximately 1.07 m/s, and approximately 0.9 m/s in the centre region.

After achieving a steady state while energizing electrodes HV2 and HV4, the configuration of the microplasma actuator was changed to HV1 and HV4 as the electrodes energized, a longer time was required to achieve a steady state for the upward flow.

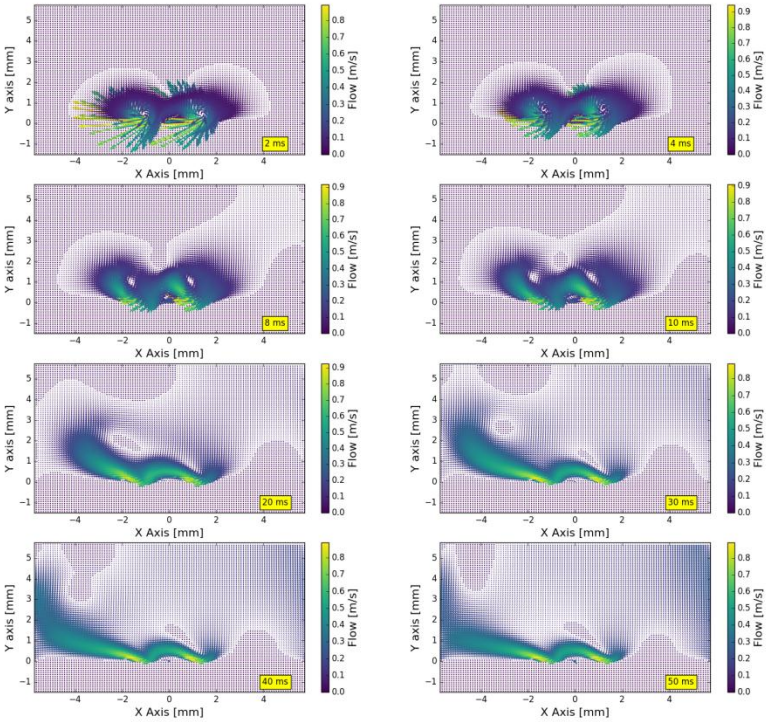

Fig. 8. Flow up to 50 ms for 4 electrodes arrangement. Electrodes HV2 and HV4 are energized at 1.4 kV.

Thus, as shown in Fig. 9 the steady state for the upward flow was achieved at approximately 120 ms.

The 4 electrodes configuration showed similar patterns for the induced flow although in the case of upward flow the complete transition from leftward flow to upward flow seems to be slower in the case of 4 electrodes configuration. The flow at 90 ms in the case of 4 electrodes configuration has still a vortex shape whilst in the case of 8 electrodes configuration the induced flow at 90 ms is almost transitioned to upward flow. In the case of energizing HV2 and HV4 electrodes leftward flow was achieved and in the configuration of the microplasma actuator with energized electrodes HV1 and HV4 upward flow was achieved.

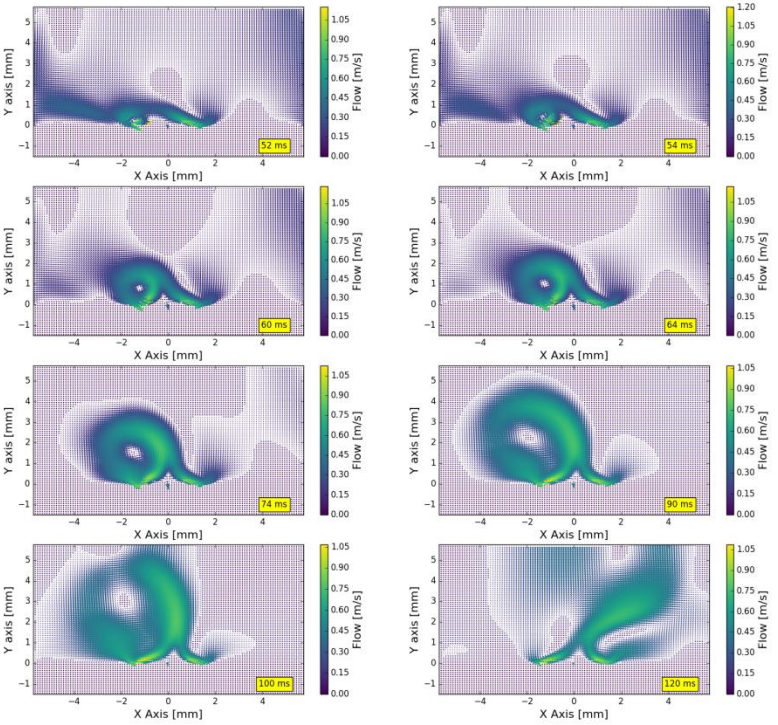

Fig. 9. Flow up to 120 ms for 4 electrodes arrangement. Electrodes HV1 and HV4 are energized at 1.4 kV.

The 8 electrodes configuration the values of the induced flow were higher than in the case of 4 electrodes configuration.

IV. Conclusion

A parametric study of microplasma actuator was carried out using numerical simulations. Thus 4 and 8 strip-like electrodes were used and their influence on the induced EHD flow was analyzed. The following conclusions were obtained:

The induced flow direction can be changed by changing the configuration of active electrodes thus from the induced leftward flow up to 50 ms a transition was made to upward flow.

With the increase of the number of active electrodes the values of the induced flow are increasing.

In both cases with 4 and 8 electrodes configuration the induced flow patterns were similar but with a slower complete transition from leftward flow to upward flow in the case of 4 electrodes configuration.

References

[1] M. Gadelhak, Flow Control. Cambridge, U.K.: Cambridge Univ. Press, 2000.

[2] J. R. Roth and X. Din, "Optimization of the aerodynamic plasma actuator as an electrohydrodynamic (EHD) electrical device," in Proc. 44th AIAA Aerospace Sci. Meeting Exhibit., Jan. 9–12, 2006, doi: 10.2514/6.2006-1203.

[3] K. P. Singh and S. Roy, "Impedance matching for an asymmetric dielectric barrier discharge plasma actuator," J. Appl. Phys., vol. 103, p. 013305, 2008.

[4] M. Neumann, C. Friedrich, J. Kriegseis, S. Grundmann, and J. Czarske, "Determination of the phase-resolved volume force produced by a dielectric barrier discharge plasma actuator," J. Phys. D: Appl. Phys., vol. 46, p. 042001, 2013.

[5] J. D. Jacob, K. Ramakumar, R. Anthony, and R. B. Rivir, "Control of laminar and turbulent shear flows using plasma actuators," in Proc. 4th Int. Symp. Turbulence Shear Flow Phenomena, Jun. 27–29, 2005.

[6] S. Im, H. Do, and M. A. Cappelli, "Dielectric barrier discharge control of a turbulent boundary layer in a supersonic flow," Appl. Phys. Lett., vol. 97, p. 041503, 2010.

[7] B. Goksel et al., "Pulsed plasma actuators for separation flow control," in Proc. Conf. Turbulence Interactions, 2006, doi: 10.13140/RG.2.1.2275.5925.

[8] F. O. Thomas, Al. Kozlov, and T. C. Corke, "Plasma actuators for bluff body flow control," J. AIAA, vol. 46, no. 8, pp. 1921–1931, 2008.

[9] Y. Li, X. Zhang, and X. Huang, "The use of plasma actuators for bluff body broadband noise control," Experiments Fluids, vol. 49, pp. 367–377, 2010.

[10] F. O. Thomas, Al. Kozlov, and T. C. Corke, "Plasma actuators for cylinder flow control and noise reduction," J. AIAA, vol. 46, no. 8, pp. 1921–1931, 2008.

[11] Y. B. Suzen, P. G. Huang, J. D. Jacob, and D. E. Ashpis, "Numerical Simulations of Plasma Based Flow Control Applications," 35th Fluid Dynamics Conference and Exhibit, June 6-9, 2005, Toronto, Ontario, AIAA 2005-4633.

[12] Y. B. Suzen, P. G. Huang, D. E. Ashpis, "Numerical Simulations of Flow Separation Control in Low-Pressure Turbines using Plasma Actuators," 45th AIAA Aerospace Sciences Meeting and Exhibit, 8 - 11 January 2007, Reno, Nevada, AIAA 2007-937.

[13] D. M. Orlov, "Modelling and Simulation of Single Dielectric Barrier Discharge Plasma Actuator," PhD Thesis, University of Notre Dame, 2006.

[14] T. Unfer, J. P. Boeuf, "Modeling of a nanosecond surface discharge actuator" J. Phys. D: Appl. Phys. 42, 194017, 2009.

[15] A. V. Likhanskii, M. N. Shneider, S. O. Macheret, R. B. Miles, "Modeling of dielectric barrier discharge plasma actuator in air", J. Appl. Phys. 103, 053305, 2008 .

[16] H. Nishida, T. Abe, "Numerical Analysis for Plasma Dynamics in SDBD Plasma Actuator", 41st Plasma dynamics and Lasers Conference, 28 June – July 1, 2010.

[17] J. Bai, J. Sun, Q. Zhang, D. Wang, "PIC simulation of RF hydrogen discharges in a transverse magnetic field," Current Applied Physics, 11 (2011) S140-S144.
[18] O. Mahfoze, S. Laizet, "Skin-friction drag reduction in a channel flow with streamwise-aligned plasma actuators," International Journal of Heat and Fluid Flow 66, 83-94, 2017.
[19] M. Blajan, Y. Mizuno, A. Ito, and K. Shimizu, "Microplasma Actuator for EHD Induced Flow," IEEE Transaction on Industry Applications, Vol. 53, No. 3, May/June 2017, pp. 2409-2415.
[20] K. Shimizu, Y. Mizuno and M. Blajan, "Basic study on force induction using dielectric barrier microplasma array," Jpn. J. Appl. Phys., Vol. 54, 01AA07, 2015.
[21] M. Blajan, A. Ito, J. Kristof and K. Shimizu, "Directional Flow Control with Multi-Electrode System Microplasma Actuator," J Biomed Syst Emerg Technol 4: 116, 2017